Journal of Thermal Analysis and Calorimetry (2022) 147:1469–1486
https://doi.org/10.1007/s10973-020-10465-9

Design and analysis of a hybrid solar power plant for co-production of electricity and water: a case study in Iran

E. Rafat[1] · M. Babaelahi[1] · A. Arabkoohsar[2]

Received: 5 August 2020 / Accepted: 1 December 2020 / Published online: 5 January 2021

Abstract
The pace of implementing solar thermal power plants is increasing all around the world. In many cases, solar plants are installed in arid areas with severe demand for potable water despite the large availability of seawater. Thus, the solar thermal power plant is combined with a thermal desalination unit for the cogeneration of electricity and sweat water. Iran is a country with a very strong potential for solar projects, and of course, under an intense crisis of water. Shiraz plant is one of the solar thermal power plants in operation in Iran. The plant has recently gone under an expansion project to be combined with a gas-fired boiler, aiming to double its capacity yet smoothening its power output. This study investigates the feasibility of the co-production of electricity–water in this case study based on a number of innovative methods in conventional and modified configurations. All the proposed scenarios are designed, thermodynamically modeled, and analyzed. The different configurations are compared in terms of energy efficiency and production rate. The results indicate that the combined cycle with heat supply through the condenser of the power block, as well as the heat recovery unit allocated for the gas boiler, outperforms all the other possible configurations. In this case, the average efficiency is 10.76%, and a daily freshwater production as high as 852.32 Tonne per day is possible for a 500 kW power plant.

Keywords Solar thermal power plant · Multi-effect desalination · Co-production · Thermodynamic analysis

List of symbols

MED	Multi-effect distillation
TVC	Thermal vapor compression
$\dot{Q}$	Heat transfer rate
$\dot{W}$	Work rate
$\dot{m}$	Mass flow rate
h	Enthalpy
P	Pressure
T	Temperature
U_{i}	Overall heat transfer coefficient
X	Salinity
η	Efficiency
η_{is}	Isentropic efficiency
η_{m}	Mechanical efficiency
R_{a}	Entrainment ratio
F	Feed seawater
LHV	Lower heating value of fuel
GOR	Gain ratio
BPE	Boiling point elevation
CR	Compression ratio
ER	Expansion ratio
LMTD	Logarithmic mean temperature difference
NEA	Non-equilibrium allowance
A	Heat transfer area
D	Distilled water

Subscripts

t	Turbine
p	Pump
wf	Working fluid
cw	Cooling water
s	Steam

Introduction

Today, there is a continuously upgrading trend towards the use of more and more renewable energy technologies [1]. This has even recently become a concern of the largest oil and gas exporter countries such as Iran, Qatar, and Saudi

✉ A. Arabkoohsar
ahm@et.aau.dk

[1] Department of Mechanical Engineering, University of Qom, Qom, Iran

[2] Department of Energy Technology, Aalborg University, Aalborg, Denmark

Arabia which are investing much in renewable energy systems such as solar thermal and power technologies, wind turbines, and geothermal systems [2]. One of the most popular renewable sources is solar energy, which may come into service for heat, cold, and power supply via different medium technologies [3].

Regardless of the source of energy, there is a general agreement that among all the energy sectors, the electricity sector is of higher importance not only due to the larger spot price of electricity compared to the heat and cold but also due to the fact advanced yet large-scale electrical heat and cold suppliers are getting more cost-effective every day paving the route for dominating electricity grids among all the energy distribution systems, e.g., gas networks, district heating, and cooling [4]. That is why renewable power production technologies have also been of much interest to the researchers and companies working in this area. This includes both solar photovoltaic and solar thermal power plants, wind farms, etc. [5]. Evidently, solar power plants are more appropriate for locations with higher solar irradiation potential, such as arid areas. These areas, most of the time, have challenges to have access to the resources of potable water. As solar desalination techniques have reached a mature state-of-practice, it is a wise idea to make a combined solar plant for the co-production of electricity and water [6]. This will certainly result in much better cost-effectiveness compared to the cases of either a solar electricity plant or a solar desalination plant working individually [7].

The combination of photovoltaic farms with reverse osmosis water desalination units and solar thermal plants with multi-effect desalination (MED) systems are the two main approaches making this happen [8]. There are several references in the literature studying such solar co-production plants in different aspects, including feasibility studies, optimization approaches, control system development of the plants, etc. [9]. Kabeel et al. [10] experimentally evaluated the integration of PV and solar still desalination for continuous water desalination. The review article presented by Khan et al. [11] gives detailed information about the methods and state of the art of photovoltaic plants combined with reverse osmosis desalination units. The main focus of this study is, however, on the hybridization of a solar thermal power plant with a thermal desalination system. There is a quite rich literature for this technology as well.

Mohammadi et al. [12] have presented a thorough review of solar concentrating power plants hybridized with thermal desalination systems. They discuss different ways of making this combination happen and address the gaps in this field to make such combined technologies broadly commercialized. Sahoo et al. [13] discussed hybrid solar–biomass power plants capable of polygeneration of cold, heat, power, and desalinated water with the case study of India. They found such a hybrid configuration much efficient for overcoming the challenge of dispatching the changeable energy output of the solar part, to decrease the cost of power supply and to contribute to reducing the level of greenhouse gas emissions in India. Sankar et al. [14] investigated techno-economically the combination of solar concentrating power plants with MED systems. They concluded that the cost of production of the hybrid system could be reduced with better use of the turbine and the generator of the power block, found the MED unit not only extremely efficient and much suitable for the production of seawater and salt but also very effective in reducing the capital cost of the plant. Ghenai et al. [15] studied the optimized design of a grid-connected solar power plant used for cogeneration of electricity and desalinated water and found the combined system economical and, of course, with much potential for emission reduction. Sorgulu et al. [16] analyzed the integration of a solar tower with thermal energy storage for the cogeneration of power and water. They studied the usage of molten salt as the thermal energy storage material and MED and RO unit for desalination of seawater and performed energy and exergy analysis to evaluate the performance of the plant. Palenzuela et al. [17] investigated a wide range of possible configurations for hybrid solar parabolic-trough plants with thermal desalination systems for arid lands and found a low-temperature MED supplied via the condenser and steam extraction from the low-pressure turbine of the solar concentrating plant quite efficient compared to other solutions. Farsi et al. [18] evaluated the performance of an integrated MED/membrane desalination system for multigeneration in a geothermal power plant to use the waste heat of the plant for the production of freshwater. The results show that the condenser in the MED system and the membrane module have the most irreversibility in the desalination unit. Trieb et al. [19] assessed the feasibility of combined solar thermal electricity-desalinated water production plants for the Mediterranean and presented instruments for enhanced project assessment using remote sensing technologies and geographic information systems. Safari et al. [20] combined a multi-effect desalination system and PEM electrolyzer with a biomass-driven power generation system for the multigeneration of electricity, freshwater, heating, and hydrogen. The performance of their proposed cycle regarding the energy and exergy efficiencies was 63% and 40%, respectively. Hasan et al. [21] modeled an IGCC power plant using waste tires as fuel for the multigeneration of power, hydrogen, and desalination. They used a Brayton and Rankine cycle for the generation of electricity and a MED unit for the desalination of water. The net power output of their proposed cycle was 7.6 MW and 6.9 MW for Brayton and Rankine cycle, and the desalination rate was 1 kg s^{-1}. Ghasemiasl et al. [22] investigated and optimized the exergetic and economic of a solar-based power and water cogeneration system. The result of their work shows a growth of 1.74%

increase in the exergy efficiency of the cycle after optimization. Hajibashi et al. [23] proposed a new procedure for the optimization of a solar-driven gas and steam combined power plant in terms of energy, exergy, and risk analysis. The thermal, exergy, and risk performance of their system is improved by 10.7%, 10.2%, and 1.21%, respectively, after the optimization. Lorente et al. [24] discussed the general tradeoffs that underpin the design of solar thermal power-water production and distribution plants and concluded that the larger the solar power-desalination plant is, the more efficient and cost-effective it can be. Mehrpooya et al. [25] presented a thermodynamic and economic analysis of an innovative hybrid multigeneration solar thermal system for the trigeneration of power, cold, and desalinated water. Their hybrid system at peak load produced about 4630 kW power, 820 kW cold, and 23 kg s^{-1} water at an overall exergy efficiency of approximately 66%. Torres et al. [26] investigated the feasibility of solar thermal power-water production plants based on the conditions of the two case studies of Venezuela and Chile and showed that such a combined plant with a capacity of 50 MWe could generate enough electricity and freshwater to feed over 85,000 people. Coppiters et al. [27] studied the feasibility of a cogeneration system including a solar hybrid micro gas turbine and multi-effect desalination unit and analyzed different design strategies of the desalination unit. The results of their work show that the cost per produced freshwater ranges from 1.78 $ to 1.92$ per cubic meter of distilled water per day which is lower than solar-powered desalination plants. Casimiro et al. [28] presented an analysis of a hybrid MED system coupled with a concentrating solar power plant in TRNSYS.

In this study, the feasibility of using the waste heat of small-scale power plants for the production of freshwater is investigated and the Shiraz power plant is analyzed as a case study for evaluation of different configurations of cogeneration. Shiraz Solar thermal power plant is a small-scale plant (only 250 kW) in operation in Iran. This Rankine-based plant works using the heat supplied via a field of parabolic trough solar collectors. This plant has recently gone under an expansion project via adding a gas-fired boiler to not only make the power output of the solar plant uniform (and consequently dispatchable) but also double its capacity. Considering the fact that Iran is experiencing a severe water crisis at the moment, this work proposes the hybridization of this combined gas–solar thermal power plant with a multistage seawater desalination unit for cogeneration of power and freshwater. Although the case study is on a small-scale, the positive outcomes of this investigation will be a reliable proof for the justification of such hybrid systems in large-scale for the utilization of the huge solar irradiation potential of the country as well as addressing its water crisis. The article investigates a wide range of possible cogeneration configurations of the plant in its conventional design and the new planned scheme. These hybridization scenarios for cogeneration of power and water include using the waste heat in the condenser, recovering the waste heat of both condenser and the auxiliary burner, and using only the waste heat of the auxiliary burner in the desalination unit. A thorough thermodynamic analysis of all the possible layouts is presented, and the different scenarios are compared in terms of efficiency and production rates and at the end, the best scenario of waste heat recovery and hybridizing the solar power plant with the desalination unit is selected and optimized using a multi-objective approach.

System description and different scenarios

As mentioned, the objective of this work is to investigate the feasibility of making Shiraz solar power plant a water–electricity cogeneration plant via the use of waste heat flows of the plant for driving a MED with thermal vapor compression (MED-TVC) unit. For this, a number of different scenarios are considered, the mathematical formulations of each of the cases are developed, the simulations are carried out, and the results are compared in terms of power generation efficiency, the amount of desalinated water, and the gain ratio of the desalination unit. This section gives information about the case study power plant and the various scenarios taken into account.

The case study

Shiraz solar power plant, located in Iran, includes a steam Rankine cycle powered by 48 parabolic solar collectors and an auxiliary boiler. The solar only configuration of the plant is capable of generating 250 kW of electricity, which is increased to 500 kW by adding the auxiliary boiler. This power plant uses both parabolic solar collectors and auxiliary burner for steam generation. This steam is then expanded in the steam turbine for the production of electricity. The outlet stream of the steam turbine is separated into two flows. The first flow goes to the condenser to be condensed and then enter the deaerator with the second flow to remove oxygen and other dissolved gases from the condensed water before being pressurized to 2120 kPa by the pump. Then, the stream gets separated again, one going to the auxiliary boiler to generate steam directly, and the other to be preheated first in the economizer and then be evaporated/superheated. Finally, the two streams are mixed to create a constant flow with 2100 kPa pressure and 532.15 K temperature at the inlet of the steam turbine. Figure 1 illustrates the schematic of the plant. The specifications of parabolic trough collectors used in the Shiraz power plant are presented in Table 1 [29, 30].

The design parameters of the plant are summarized in Table 2 [31].

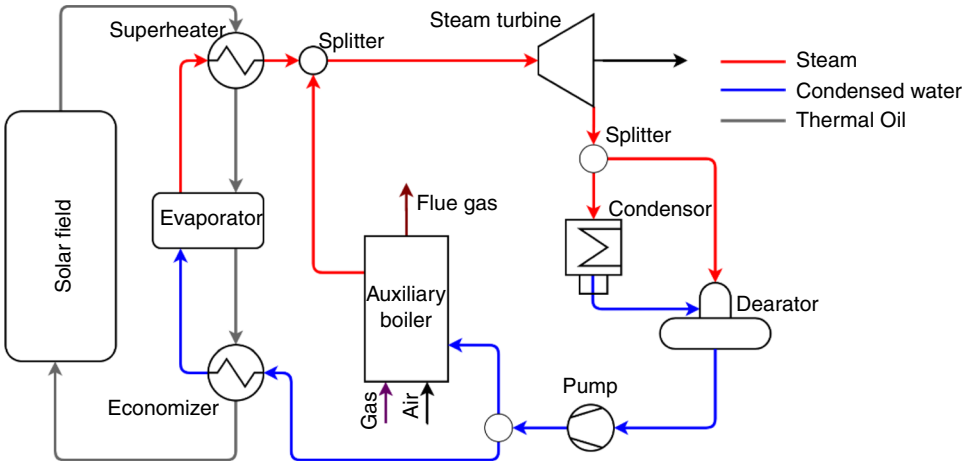

Fig. 1 Schematic of the Shiraz power plant (case 1)

Table 1 Solar collectors' specifications

Parameter	Value	Parameter	Value
Length	25 m	Reflectivity of mirror	0.873
Width	3.4 m	Transmissivity of cover	0.96
Aperture	3.1 m	Emissivity of cover	0.25
Focal length	88 cm	Absorptivity of receiver	0.94
Outer diameter of the receiver	7 cm	Emissivity of the receiver at 300 °C	0.14
Outer diameter of cover	12.5 cm	Intercept factor	0.93
Collector heat removal factor	0.98	Maximum optical efficiency	0.78
Concentration ratio	14	Rim angle	90°

Table 2 Shiraz power plant thermodynamic parameters

Parameter	Value
Power generation	500 kW
Steam turbine inlet temperature	532.15 K
Steam turbine inlet pressure	2100 kPa
Steam turbine outlet pressure	130 kPa
Outlet temperature of solar collector	538.4 K
Turbine isentropic efficiency	58%
Condensate pump isentropic efficiency	30%

The hybrid configurations

For accomplishing the feasibility study of hybridizing the Shiraz solar power plant with a desalination unit in this work, five different scenarios (or configurations) are considered to be analyzed to find the best possible solution. First, the base case without the desalination unit is investigated to examine the performance of the conventional cycle (Fig. 1).

Shiraz power plant has a turbine outlet pressure of 130 kPa which makes it suitable to be used directly as the motive steam in the MED unit. This situation is studied as the second scenario (case 2) to recover the heat wasted in the condenser for water desalination (Fig. 2).

In case 3, waste heat from both the turbine outlet stream and the auxiliary boiler is used to generate the motive steam used in the MED unit (Fig. 3).

The fourth configuration (case 4) investigates the condition where only the heat from the auxiliary boiler exhaust gas is used in the MED unit (Fig. 4). This case is analyzed in order to understand the possibility of producing freshwater using only the exhaust of the boiler, in case recovering the waste heat of the condenser was not accessible.

Finally, as the last scenario (case 5), the possibility of desalination in the solar only plant, when there is no auxiliary boiler, is assessed (Fig. 5).

Mathematical model

In this section, a mathematical model is provided for the thermodynamic analysis of the proposed power plant and solar power-MED plant.

Power plant

A control volume is considered around each component to develop energy equations for the thermodynamic modeling of the system. Neglecting the potential and kinetic terms,

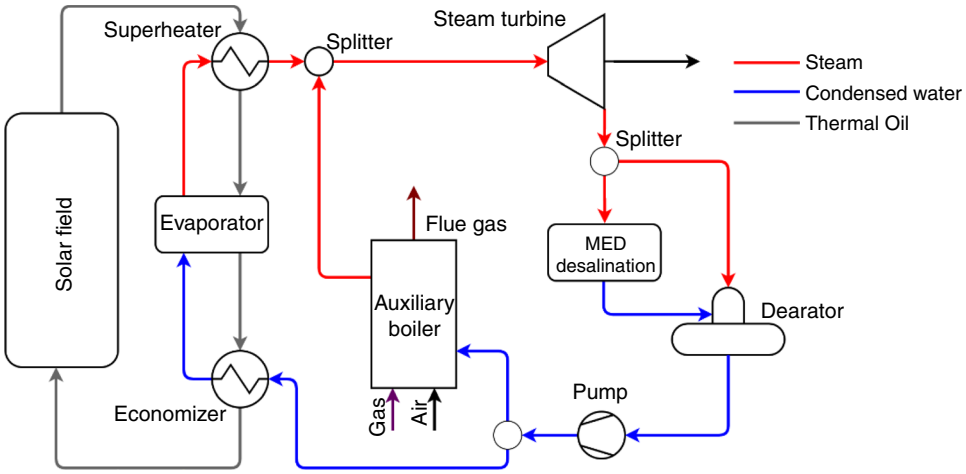

Fig. 2 Schematic of the Shiraz power plant hybrid with a desalination unit (case 2)

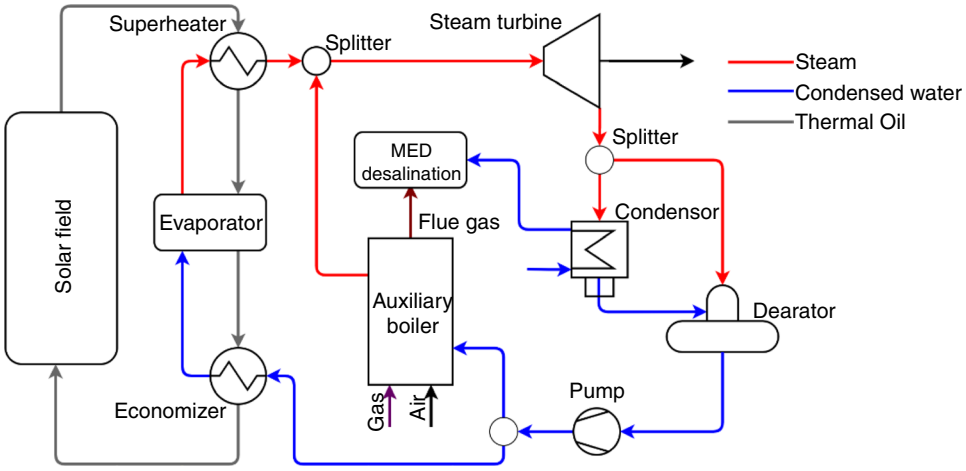

Fig. 3 Both waste heat of the condenser and that of the auxiliary boiler are used in the desalination unit (case 3)

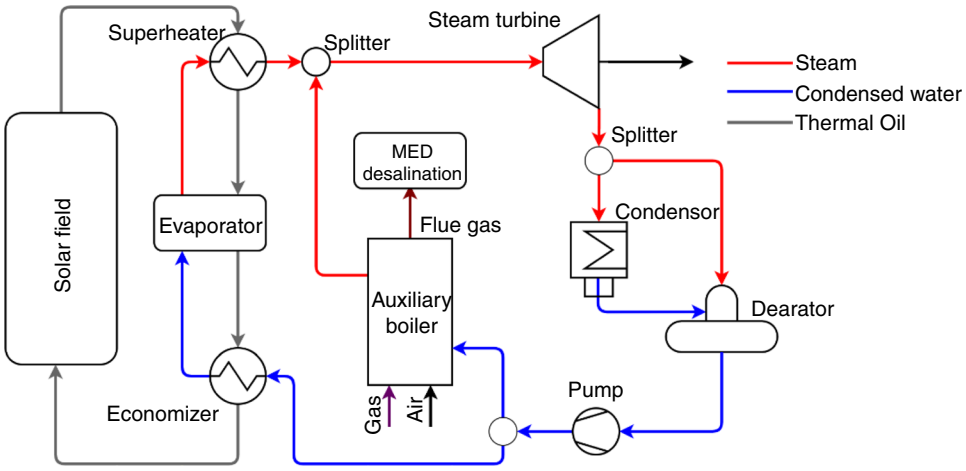

Fig. 4 Only the heat from exhaust gases is used to generate the motive steam used in the MED unit (case 4)

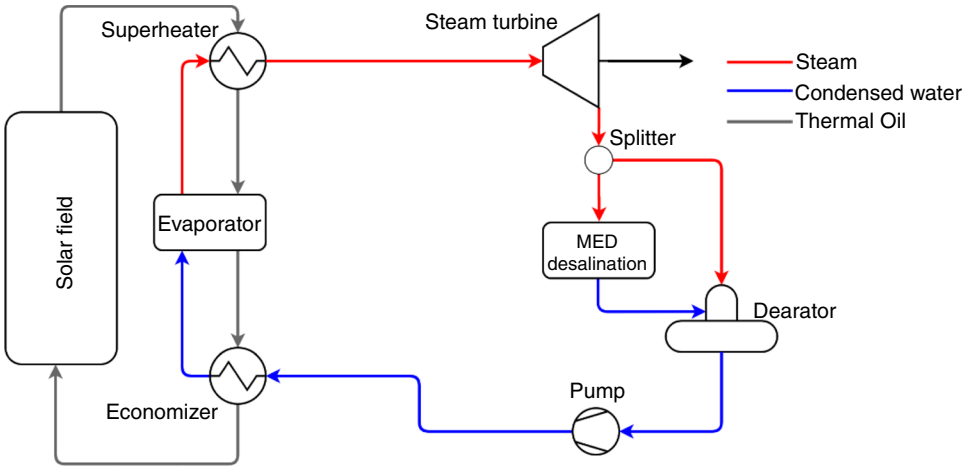

Fig. 5 Schematic of the solar-only plant hybrid with a desalination unit (case 5)

the energy balance of any open control volume will be as follows [32]:

$$\dot{Q}_{\text{net,in}} - \dot{W}_{\text{net,out}} = \sum_{\text{out}} \dot{m}h - \sum_{\text{in}} mh + \left(m_2 u_2 - m_1 u_1\right)_{\text{system}} \tag{1}$$

where h and u are the specific enthalpy and the internal energy, m and $\dot{m}$ are mass of the control volume and mass flow rate, and $\dot{Q}$ and $\dot{W}$ are the heat transfer rate and net output work rate, respectively.

The mass balance of each component is as [33]:

$$m_2 - m_1 = \sum \dot{m}_{\text{in}} + \sum \dot{m}_{\text{out}} \tag{2}$$

Considering the general mass and energy balance equations above, Table 3 lists the required correlations for energy analysis of the entire system.

The energy efficiency of the plant is calculated from [35]:

$$\eta = \frac{\dot{W}_{\text{net,out}}}{\dot{m}_{\text{f}} \times \text{LHV} + Q_{\text{Solar}}} \tag{9}$$

where $\dot{W}_{\text{net,out}}$ is the net power generation of the plant, $\dot{m}_{\text{f}}$ and LHV are the mass flow rate and the lower heating value of the fuel used in the auxiliary boiler, and Q_{Solar} is the heat absorbed by the fluid in the parabolic trough collectors.

Table 3 Energy balance equations of the power plant components [34]

Component	Equation	
Steam turbine	$\dot{W}_{\text{t}} = \dot{m}\left(h_{\text{in}} - h_{\text{out}}\right)\eta_{\text{m,t}}; \eta_{\text{is,t}} = \frac{\dot{W}_{\text{t}}}{\dot{W}_{\text{is,t}}}$	(1)
Pump	$\dot{W}_{\text{p}} = \frac{\dot{m}\left(h_{\text{out}} - h_{\text{in}}\right)}{\eta_{\text{m,p}}}; \eta_{\text{is,p}} = \frac{\dot{W}_{\text{is,p}}}{\dot{W}_{\text{p}}}$	(2)
Heat exchangers	$\dot{m}_{\text{wf}}(h_{\text{wf,out}} - h_{\text{wf,in}}) = \dot{m}_{\text{oil}}\left(h_{\text{oil,in}} - h_{\text{oil,out}}\right)$	(3)
Condenser	$\dot{m}_{\text{wf}}(h_{\text{wf,in}} - h_{\text{wf,out}}) = \dot{m}_{\text{cw}}\left(h_{\text{cw,out}} - h_{\text{cw,in}}\right)$	(4)
Deaerator	$\dot{m}_{\text{w}} h_{\text{w,in}} + \dot{m}_{\text{s}} h_{\text{s,in}} = \left(\dot{m}_{\text{w}} + \dot{m}_{\text{s}}\right) h_{\text{w,out}}$	(5)
Auxiliary boiler	$Q_{\text{boiler}} = \dot{m}\left(h_{\text{s,out}} - h_{\text{w,in}}\right)$	(6)

Multi-effect desalination unit

The schematic of a MED-TVC system is illustrated in Fig. 6 . Energy balance equations are applied to vapor effects, TVC, flash chambers, and the condenser for modeling the system. The input parameters of the modeling include the temperature of the top brine, boiling temperature of the last effect, total feed flow rate, motive steam flow rate, cooling water temperature, the temperature of the inlet seawater, salinity of the inlet, motive steam pressure, and the number of effects [36].

The temperature difference along the effects (i.e., desalination stages) is assumed to be equal, which is calculated as below, where T_1 and T_n are the temperature in the first and last effects and n is the number of effects [37]:

$$\Delta T = \frac{T_1 - T_n}{n - 1} \tag{10}$$

The compressed steam temperature can be calculated as follows:

$$T_s = T_1 + \Delta T \tag{11}$$

The temperature of the vapor in the last effect is obtained from:

$$T_{V_n} = T_n - \text{BPE} \tag{12}$$

Boiling point elevation (BPE) is the increase in the boiling temperature of the water because of the dissolved salts and is calculated by [38]:

$$\text{BPE} = Xb \times (B + (C \times Xb)) \times 10^{-3} \tag{13}$$

where

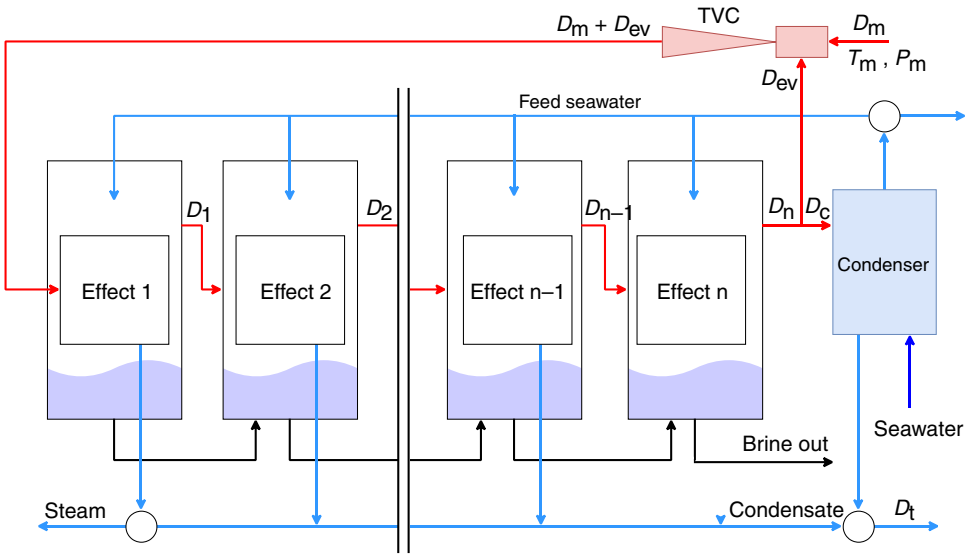

Fig. 6 Schematic of a MED-TVC system

$$B = \left(6.71 + 6.34 \times T_n \times 10^{-2} + 9.74 \times T_n^2 \times 10^{-5}\right) \times 10^{-3}$$
$$C = \left(22.238 + 9.59 \times T_n \times 10^{-3} + 9.42 \times T_n^2 \times 10^{-5}\right) \times 10^{-8}$$

The following equation is used to obtain the heat capacity of water:

$$C_P = \left(a + b \times T + c \times T^2 + d \times T^3\right) \times 10^{-3} \tag{14}$$

In which,

$$a = 4206.8 - 6.6197 \times S + 1.2288 \times S^2 \times 10^{-2}$$
$$b = -1.1262 + 5.4178 \times S \times 10^{-2} - 2.2719 \times S^2 \times 10^{-4}$$
$$c = 1.2026 \times 10^{-2} - 5.3566 \times S \times 10^{-4} + 1.8906 \times S^2 \times 10^{-6}$$
$$d = 6.8777 \times 10^{-7} + 1.517 \times S \times 10^{-6} - 4.4268 \times S^2 \times 10^{-9}$$

And,

$$S = X_f \times 10^{-3}$$

Compressed steam pressure (P_s) and entrained steam pressure (P_{ev}) can be calculated from the correlation proposed by Ettouney and El-Dessouky as [39]:

$$P_s = 10^3 \times \exp\left(\frac{-3892.7}{T_s + 273.15 - 42.6776} + 9.5\right) \tag{15}$$

$$P_{ev} = 10^3 \times \exp\left(\frac{-3892.7}{T_{v_n} + 273.15 - 42.6776} + 9.5\right) \tag{16}$$

Compression ratio (CR) and expansion ratio (ER) are, respectively, given by:

$$\mathrm{ER} = \frac{P_m}{P_{ev}} \tag{17}$$

$$\mathrm{CR} = \frac{P_s}{P_{ev}} \tag{18}$$

where P_m, P_s, and P_{ev} represent the motive steam temperature, compressed vapor pressure, and the entrained vapor pressure, respectively.

The following equation can be used to evaluate the entrainment ratio (R_a) and the amount of entrained vapor (D_{ev}) [40]:

$$R_a = 0.235\left(\frac{P_s^{1.19}}{P_{ev}^{1.04}}\right) \times \mathrm{ER}^{0.015} \tag{19}$$

$$D_{ev} = \frac{D_m}{R_a} \tag{20}$$

The temperature of vapor and brine in the ith effect may be calculated by:

$$T_{v_i} = T_i - \mathrm{BPE} \tag{21}$$

$$T_{i+1} = T_i - \Delta T \tag{22}$$

As the feed seawater (F) is equally distributed, the feed flow rate in all the effects is the same and equal to:

$$F_i = \frac{F}{n} \tag{23}$$

The brine leaving each effect can be obtained from:

$$B_1 = F_1 - D_1 \tag{24}$$

$$B_i = F_i + B_{i-1} - D_i; \quad i \geq 2 \tag{25}$$

The salinity of the brine leaving each effect is calculated as:

$$Xb_1 = \frac{F_1}{B_1} \times X_f \tag{26}$$

$$Xb_i = \frac{F_i}{B_i} \times X_f + \frac{B_{i-1}}{B_i} \times X_{i-1}; \quad i \geq 2 \tag{27}$$

The vapor in each effect is obtained as below:

$$D_1 = \frac{\left(D_m + D_{ev}\right)\lambda_s - F_1 C_P\left(T_1 - T_f\right)}{\lambda_1} \tag{28}$$

$$D_2 = \frac{D_1\lambda_1 - F_2 C_P\left(T_2 - T_f\right) + B_1 C_P\left(T_1 - T_2\right)}{\lambda_2} \tag{29}$$

$$D_i = \frac{\left(D_{i-1}\lambda_{i-1} + D'_{i-1}\right)\lambda_{i-1} - F_i C_p\left(T_i - T_f\right) - B_{i-1} C_P\left(T_{i-1} - T_i\right)}{\lambda_i}; \quad i \geq 3 \tag{30}$$

where λ is the latent heat of evaporation and is obtained as follows:

$$\lambda_i = 2589.583 + 0.9156 \times T_i - 4.834 \times 10^{-2} \times T_i^2 \tag{31}$$

And D' is the amount of vapor generated because of the flashing inside flash boxes

$$D'_i = \frac{D_{i-1} C_P\left(T_{v,i-1} - T'_i\right)}{\lambda_i} \tag{32}$$

$$T_{v,i-1} = T_i - \mathrm{BPE} \tag{33}$$

$$T'_i = T_{v,i-1} - \mathrm{NEA}_i \tag{34}$$

$$\mathrm{NEA}_i = 33 \times \frac{\left(T_{i-1} - T_i\right)^{0.55}}{T_{v,i}} \tag{35}$$

In the last effect, the vapor is divided into two parts, one going to the condenser (D_C(and the other is entrained by the TVC (D_{ev}).

$$D_C = D_n - D_{ev} \tag{36}$$

The amount of total distilled water is the sum of distillate in each effect

$$D_t = \sum_{i=1}^{n} D_i \tag{37}$$

The overall heat transfer coefficient can be calculated as below [41]:

$$U_i = \left(1939.4 + 1.40562 \times T_i - 0.0207525 \times T_i^2 + 0.0023186 \times T_i^3\right) \times 10^{-3} \tag{38}$$

Heat transfer area of the multi-effect evaporator unit is given by:

$$A_1 = \frac{\left(D_s + D_{ev}\right) \times \lambda_s}{U_1\left(T_s - T_1\right)} \tag{39}$$

$$A_i = \frac{D_i \lambda_i}{U_i\left(T_{C_i} - T_i\right)}; \quad i \geq 2 \tag{40}$$

$$A_e = \sum_{i=1}^{n} A_i \tag{41}$$

The heat transfer area of the condenser section is calculated as:

$$A_C = \frac{D_c \lambda_n}{U_c \times \mathrm{LMTD}_c}; \text{ where } \mathrm{LMTD}_c = \frac{T_f - T_{cw}}{\ln\left(\frac{T_{v_n} - T_{cw}}{T_{c_n} - T_f}\right)} \tag{42}$$

The overall heat transfer coefficient of the condenser is:

$$U_c = 1.7194 + 3.2063 \times T_{v_n} \times 10^{-2} - 1.5971 \times T_{v_n}^2 \times 10^{-5} + 1.9918 \times T_{v_n}^3 \times 10^{-7} \tag{43}$$

Specific heat transfer area is the total heat transfer area per unit distilled water:

$$A_d = \frac{A_e + A_c}{D_t} \tag{44}$$

The gain ratio is calculated to evaluate MED-TVC performance [42]:

$$\mathrm{GOR} = \frac{D_t}{D_m} \tag{45}$$

Multi-objective optimization procedure

In this paper, after the determination of the best scenario for cogeneration, an optimization process is applied to find the optimum parameters of the plant. For this purpose, a robust optimization algorithm, multi-objective genetic algorithm optimization, is employed to maximize the efficiency of the cycle as well as the freshwater distillation. In multi-objective optimization, two or more objectives are attempted to be minimized (or maximized) simultaneously within the

decision variables constraints. Figure 7 illustrates the flowchart of optimization using Genetic Algorithm.

Since the results of a multi-objective optimization is not a single optimum point and is a collection of optimum points, a decision-making process is needed for the selection of the final optimum point. In this paper, a LINMAP decision-making method is implemented for this purpose. In this method, first, all objectives points in the Pareto Frontier are normalized to become Euclidean non-dimensional values, then using the following equation, the point with the least distance to the ideal point is selected as the final optimum point. [43]

$$d = \sqrt{\sum_{k=1}^{n} \left(P_{ij} - P_{j}^{Ideal} \right)^2}$$

The objective functions, decision variables, and the range of each variable are described in Table 4.

Table 4 Decision variables and objective functions in the optimization

	Range [44]
Decision variables	
X1: Collector's outlet temperature	532–573 K
X2: Steam turbine inlet pressure	1500–3000 kPa
X3: Steam turbine outlet pressure	80–200 kPa
X4: Steam turbine inlet temperature	500–700 K
X5: Heat exchangers minimum approach temperature	5–30 K
Objective functions	
Y1: Energy efficiency	%
Y2: Distilled water	/kg s^{-1}

Results and discussion

The results of the modeling and simulations of the different considered scenarios are presented in this section.

Before presenting the results, the model used for different parts of the hybrid plant should be validated. This power plant mainly includes the solar collectors' field, the desalination system, and the power block. Apart from the model of the power block, which is based on the well-known and simple thermodynamic models, the models developed for the solar collectors and the desalination unit should be validated. The validation processes are performed comparing the results given by the developed models of this work and the experimental results available in the literature.

For the solar power plant, the validation is carried out by comparing the results associated with the collectors' field outlet temperature and steam temperature generated by the solar working fluid with those reported in Ref. [45] for the same power plant and the same operation conditions on the 22nd of June 2009 [45]. As can be seen in Fig. 8 , there is a

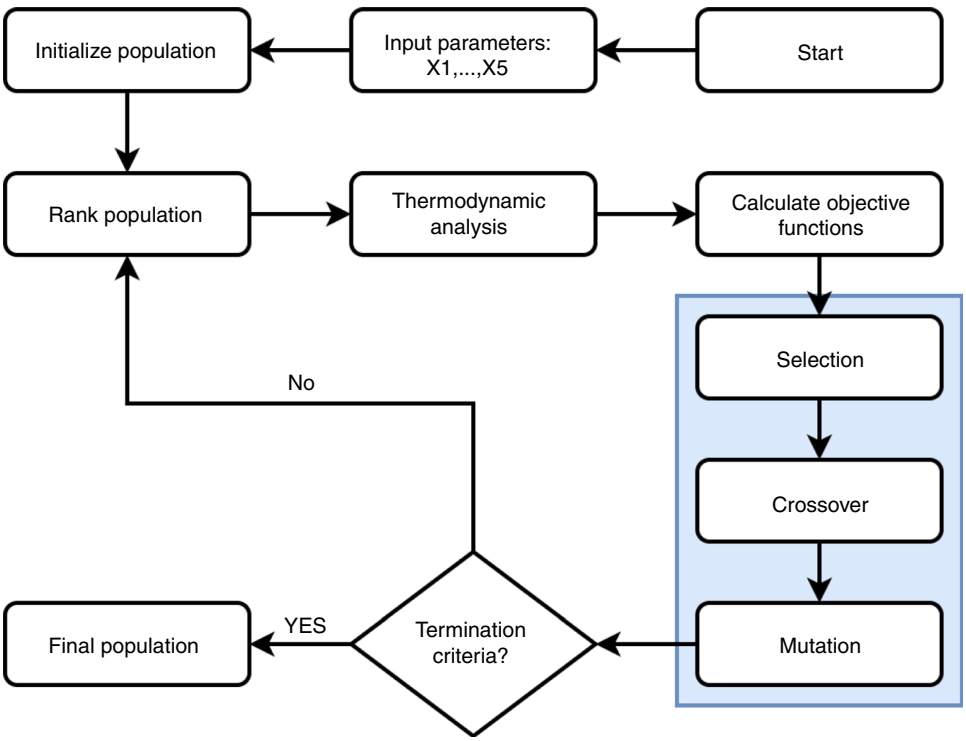

Fig. 7 Optimization procedure

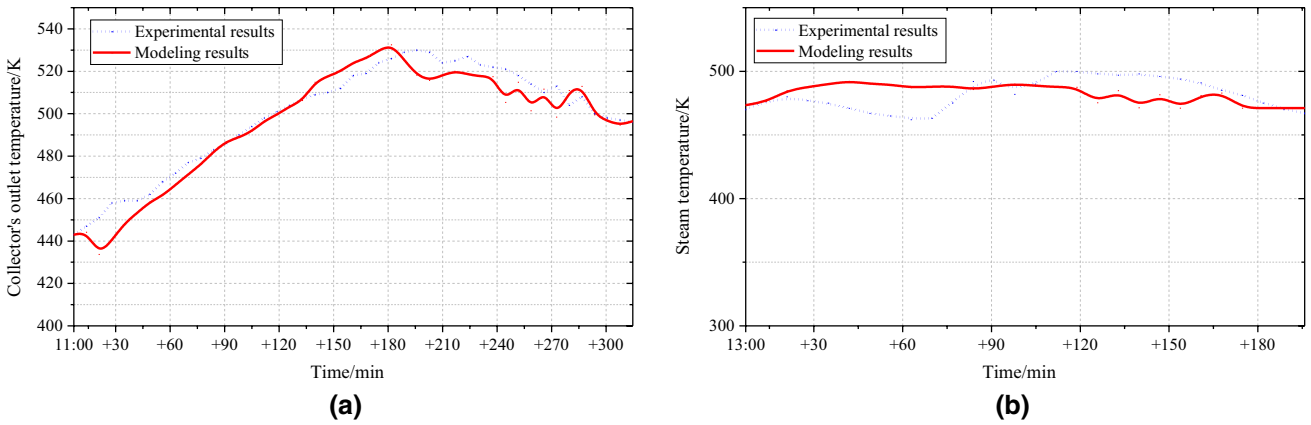

Fig. 8 Comparison of the experimental results and the modeling: a collector's outlet temperature and, b steam temperature

Table 5 Results of MED-TVC validation

Parameters	Modeling results	Reference [46]	Difference /%
Distillate production (kg/s)	50.2	52.4	4.2
Gain ratio	7.8	8.3	6.1
Cooling water flow rate (kg/s)	261.9	258.3	1.4

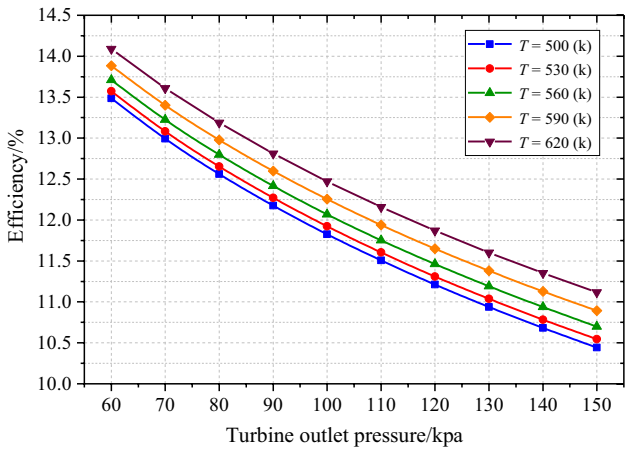

Fig. 9 Effect of turbine outlet pressure on the efficiency of the cycle with different turbine inlet temperature

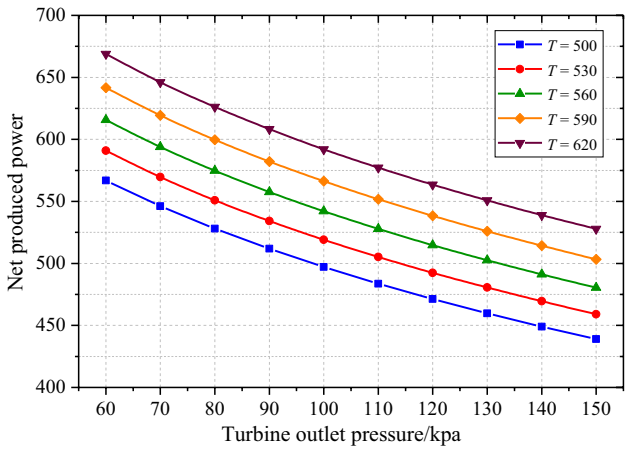

Fig. 10 Effect of turbine outlet pressure on the produced power with different turbine inlet temperatures

good agreement between the model and experimental measurements as the average difference is less than 3%.

The model for the multi-effect desalination unit is also validated with the data of the Qeshm distillation plant. The validation result of the employed mathematical model for simulating the desalination unit is presented in Table 5.

Figure 9 investigates the effects of turbine inlet temperature and outlet pressure on the efficiency of the Rankine-based power block of the case study solar power plant. According to the figure, and expectedly, by decreasing the outlet pressure, the pressure ratio of the turbine increases, which results in an increase in power production and, consequently, the efficiency of the cycle. Here, by decreasing the turbine outlet pressure to 60 kPa and increasing the inlet turbine temperature to 620 K (from the current state of 130 kPa and 530 K), an efficiency as high as 14% can be achieved.

Figure 10 assesses the effects of the same parameters in the case study on the rate of the power output of the plant. Naturally, the same trend as that seen in the previous figure is expected here. This is due to the fact that the power generation in the turbine has a direct relationship to its pressure ratio, and by decreasing the outlet pressure, thus increasing the pressure ratio of the turbine, the power generation

increases as well. As seen, in the base case ($T = 530$ K), by decreasing the outlet pressure to 60 kPa, about 110 kW more power can be generated in the steam turbine, which is a considerable number. By increasing the inlet temperature to 620 K, electricity as much as 670 kW can be achievable.

Figure 11 studies the effect of minimum approach temperature of heat exchangers on the efficiency of the power plant. A rise in this temperature difference leads to a drop in the performance of the cycle since when the heat exchanger pinch temperature increases, the temperature of the flow leaving the superheater decreases too. To overcome this temperature drop and to maintain the properties of the turbine inlet flow, the outlet temperature of the boiler needs to be increased, thus increasing the amount of fuel burned in the boiler. As a result, increasing the approach temperature of heat exchangers from 5 to 30 can decrease the efficiency of the cycle from 13.5 to a low of only 9.5.

The impact of turbine outlet pressure on the performance of the desalination unit is investigated in Fig. 12. As seen from the figure, raising the turbine outlet pressure has a mildly negative effect on the performance of the MED-TVC unit in cases 2 and 5. This is because the outlet stream of the turbine is directly used as the motive steam in these configurations. Increasing the motive steam pressure leads to a rise in the entrained vapor pressure and the expansion ratio of the system. The rise in the expansion ratio causes a growth in the entrainment ratio and also lowers the entrained vapor flow rate. This decrease in the flow rate also decreases the amount of produced desalinated water in the first effect, thus lowering the gain ratio of the MED-TVC. Since in case 3 the waste heat from the turbine outlet stream is used to generate the motive steam and the turbine outlet stream is not used directly in the desalination unit, by increasing the turbine outlet pressure, the outlet temperature increases too, and thus the amount of available heat which can be used to generate the motive steam increases too, hence increasing the motive steam mass flow which leads to an increase in the amount of distilled water and the GOR. Changes in the turbine outlet pressure do not affect the performance of case 4 as only the waste heat from the boiler is used in this configuration.

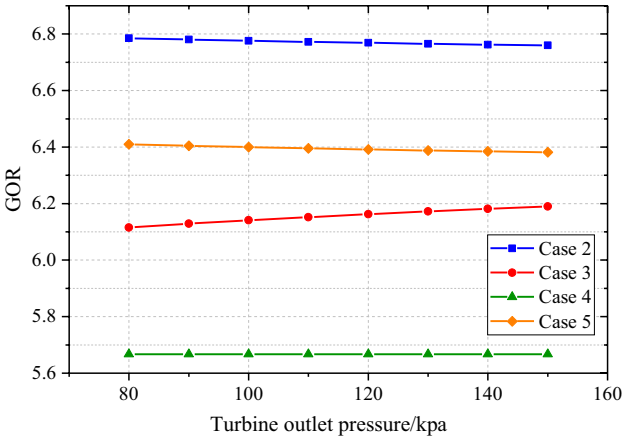

Fig. 12 Effect of the turbine outlet pressure on the gain ratio of the desalination unit

The relations between the top brine temperature, number of effects, and GOR are shown in Fig. 13. Increasing the temperature of the brine results in a fall in the GOR of the desalination unit. This is due to the fact that by raising the brine temperature, a higher pressure ratio is needed in the ejector, thus requiring more motive steam. However, the brine temperature affects the consumed heat in the unit and the heat transfer area, and the increase of the brine temperature, due to the temperature difference, has a positive effect on lowering the needed heat transfer area. The results show that by decreasing the top brine temperature, the GOR value increases gradually, as by decreasing the temperature from

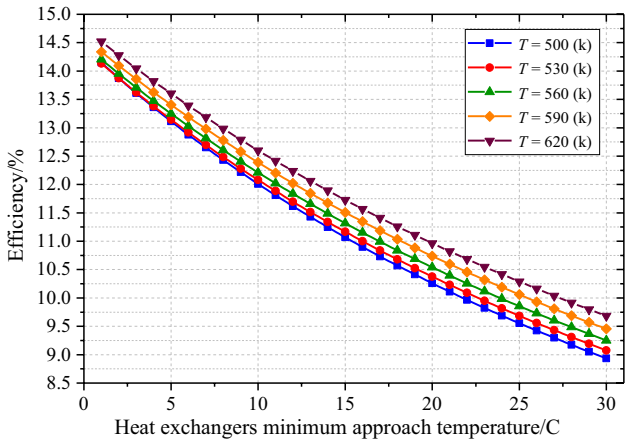

Fig. 11 Effect of heat exchangers minimum approach temperature on the performance of the cycle

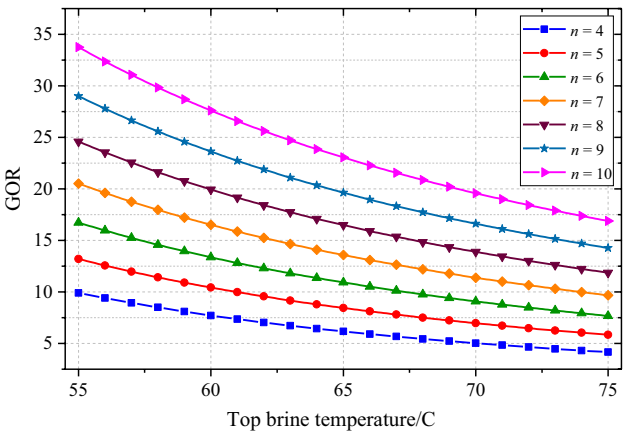

Fig. 13 Impact of the top brine temperature on the GOR in terms of different number of effects

75 to 55 °C, the GOR rises from 11.8 to 24.6. Furthermore, at a particular temperature, increasing the number of effects causes an improvement in the gain ratio. For instance, with a top brine temperature of 65 °C, doubling the number of effects from 4 to 8, leads to a ten-point increase in the GOR value. This is because by increasing the number of effects, the possibility of transferring heat between flows increases.

Figure 14 illustrates the relation between the number of effects in the MED system and the gain ratio as well as the specific heat transfer area. According to the figure, by increasing the number of effects, more heat is recovered in effects, and consequently, the gain ratio increases. On the other hand, more desalination stages (effects) mean an increased specific heat transfer area, which is, indeed, to an increase in the cost of the system. By doubling the number of effects from 4 to 8, the gain ratio of the desalination plant rises from 5.32 to 12.46. By adding the 9th effect, however, the GOR only increases by 1.38 to reach 13.85, while the specific heat area continues its exponential increase. Looking at the figure, the most significant gap between gain ratio and specific heat transfer area happens at the case when we have eight effects, making it a considerable choice.

Table 6 shows the results of the steady-state analysis of each scenario and compares the performance of each case in terms of energy efficiency, generated steam, distilled water, and gain ratio. The DNI is assumed to be 800 W m^{-2} in these calculations. The results of the steady-state analysis show that the second scenario, using the MED as the condenser has the highest performance in terms of water desalination. However, since the performance of the solar power plant changes under different solar irradiation values, an analysis considering the weather condition is needed for the selection of the best configuration.

For doing the simulations under real fluctuating available energy source for the plant, the local solar irradiation intensity over a 15-day period of the year from August 27 to September 10 (2019) is considered. Figure 15 presents the hourly average direct normal irradiation (DNI) in Shiraz during these days. As seen, the maximum DNI during the day is expected to be about 850 W m^{-2}. In addition, according to the figure, Shiraz has been quite rich in terms of solar energy availability during the sample period, as very little fluctuations are seen in the daily profiles of the DNI.

Figure 16 illustrates the fluctuations of the auxiliary boiler's fuel mass flow rate during the period of the study. Here, it is supposed that the power output of the plant at any given condition should be kept at a constant rate of 500 kW. For achieving this, as seen, during the day, with the increase of solar irradiation and as a result, the delivered heat by solar collectors, the fuel consumption in the auxiliary boiler decreases to the low point of 0.04 kg s^{-1}, and at night, when there is no available solar energy, the fuel flow rate reaches to the peak point of 0.9 kg s^{-1}.

Naturally, the plant efficiency, besides the several technical factors, is a function of solar energy availability too. The changes in the power plant efficiency as the DNI varies are shown in Fig. 17. Overall, it can be seen that the efficiency of the plant rises as solar irradiation grows, except the peak solar irradiation points at which there are small reductions in the efficiency values which are because of the oil mass flow rate in collectors reaching its maximum value, thus

Table 6 Results of the steady-state analysis

Case no	Energy efficiency/%	Generated steam/kg s^{-1}	Distilled water/kg s^{-1}	GOR
Case 1	11.126	–	–	–
Case 2	11.122	1.5358	8.7879	6.722
Case 3	11.01	0.7858	4.8504	6.1722
Case 4	11.01	0.3238	1.8347	5.6669
Case 5	10.65	0.8568	5.4503	6.3615

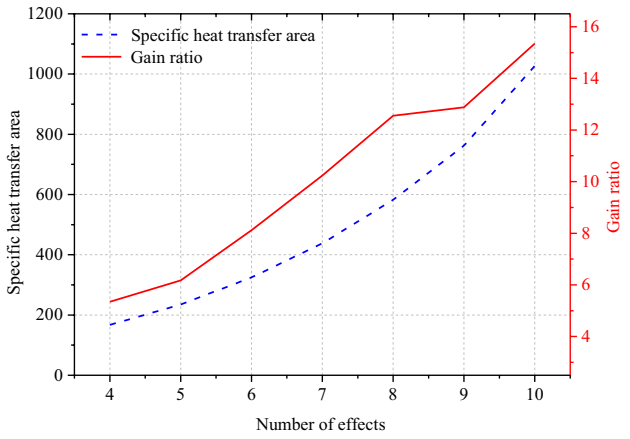

Fig. 14 Impact of the number of effects on gain ratio and heat transfer area

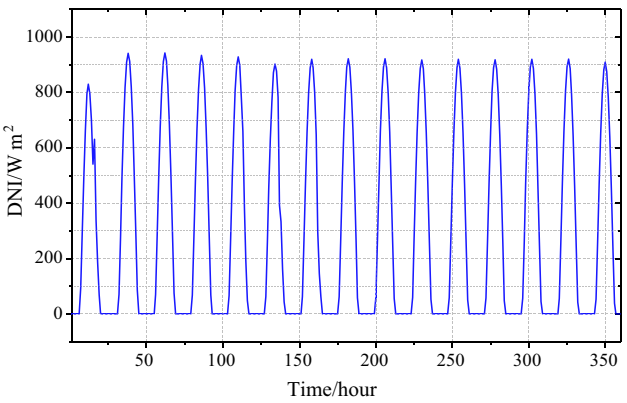

Fig. 15 Solar irradiation on a horizontal surface in the case study

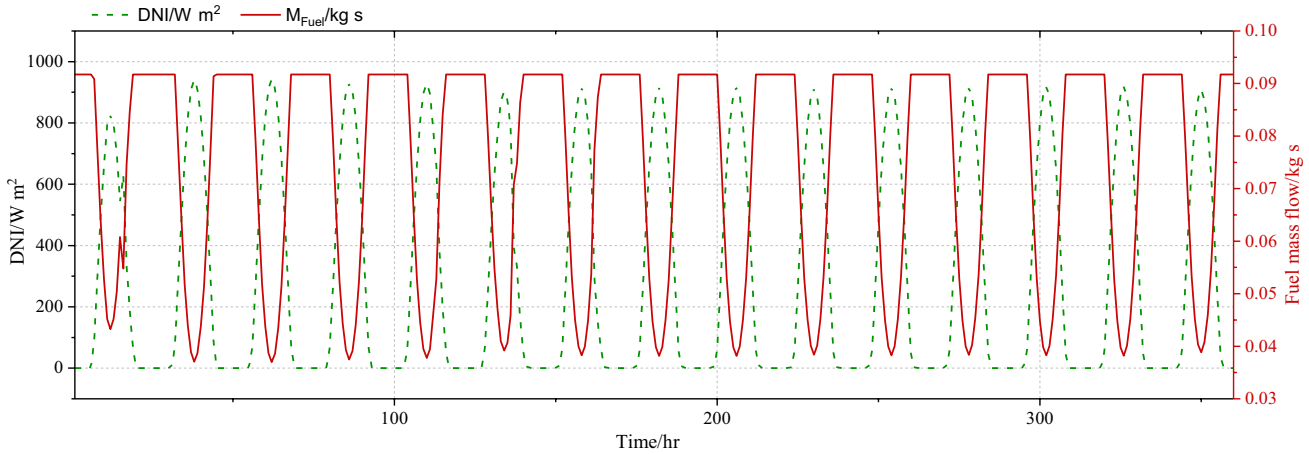

Fig. 16 Fuel mass flow rate during the considered period

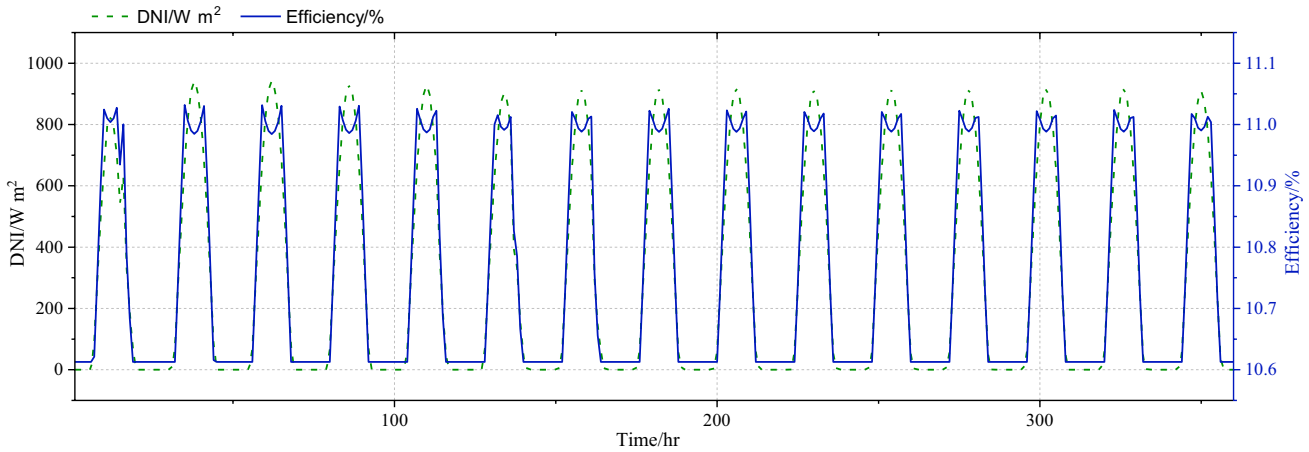

Fig. 17 Plant efficiency during the period of study

decreasing the percentage of heat recovered in the collectors. This, however, is not of significant importance as the maximum efficiency of the plant is about 11% when solar irradiation is at the highest level while the efficiency is at the minimum value of 10.6% when the solar irradiation level approaches the dead point of zero.

The relation between solar irradiation, auxiliary boiler fuel mass flow rate, and the power generation efficiency is illustrated in Fig. 18. As the solar irradiation level increases, the heat absorbed by the thermal oil in the solar collectors increases, and more steam is generated in the evaporator. Thus, less steam needs to be provided, resulting in a reduction in the fuel mass flow rate since the power output of the plant is considered to be constant, which results in a rise in the efficiency of the cycle. It can be seen that while DNI fluctuates between 0 and 850 W m^{-2}, the efficiency changes between 10.65 and 11.05%, and the fuel rate varies between 0.035 and 0.09 kg s^{-1}.

The amount of distilled water in different configurations of the hybrid power plant is illustrated in Fig. 19. In case 2, the MED unit is set to be after the turbine and in the condensing section. Since the production of the plant is controlled to be fixed at 500 kW, when solar irradiation decreases, fuel mass flow increases in the auxiliary boiler, so the properties of the fluid at the inlet of the turbine do not change. As a result, the turbine outlet properties and the heat transferred to the desalination unit remain the same, so the production of desalinated water remains constant too. Case 2 represents the situation where both heat from the turbine outlet stream and auxiliary boiler exhaust gases are used for the generation of motive steam in the desalination unit. In this case, with the decrease of solar share, the shortage of heat in the plant will be resolved in the auxiliary boiler by increasing the fuel flow rate, which results in an increase in the exhaust flow rate. In this way, the heat transferred to the MED unit increases, thus increasing the production

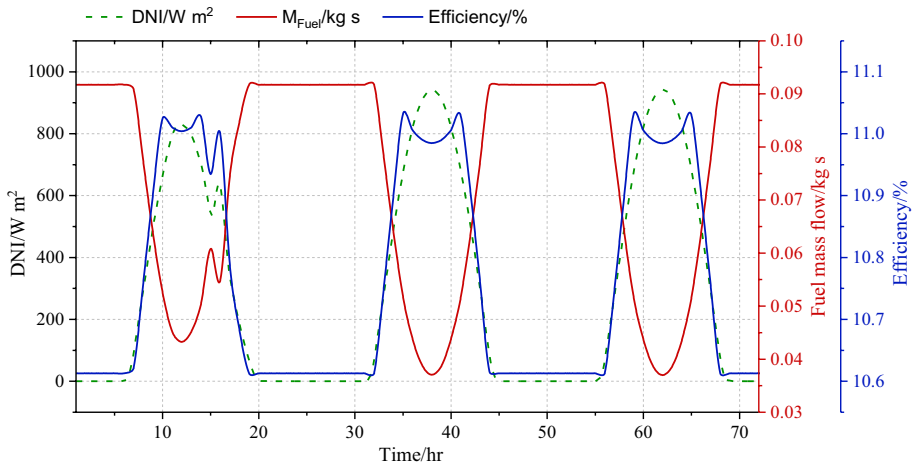

Fig. 18 Comparison of efficiency and fuel flow rate changes in the first 3 days

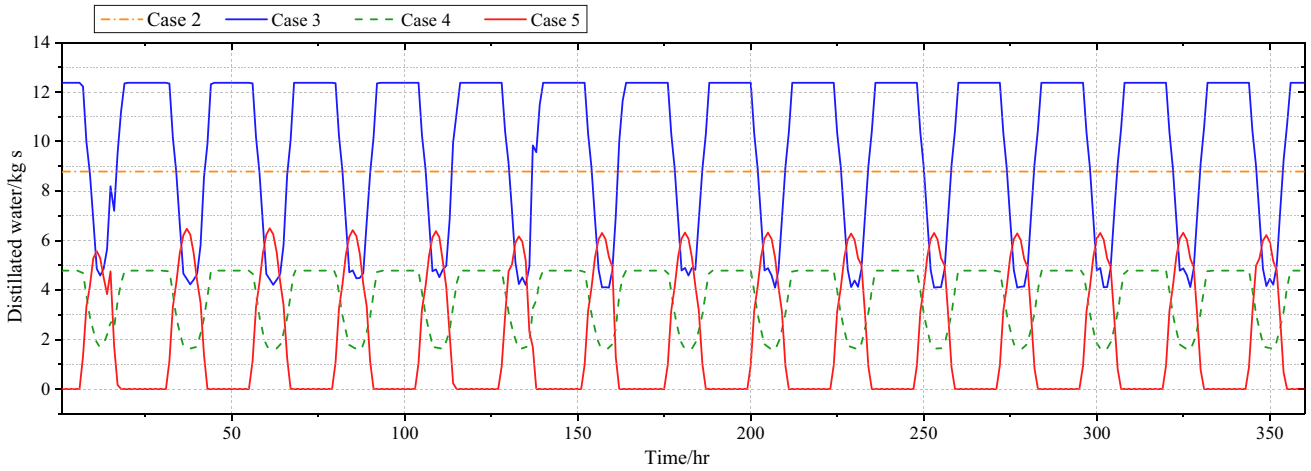

Fig. 19 Amount of distillation in different cases

of distillate water. In case 4, only the waste heat from the auxiliary boiler is used to produce desalinated water. Similar to case 2, by the increase of fuel mass flow rate, the water production increases too but is generally lower than case 2, as can be expected. The hybridization of the desalination unit with the solar only cycle is presented in case 5. In this case, the properties of the turbine inlet stream change during the day, as there is no auxiliary boiler to control the temperature by increasing the fuel flow rate. Thus, the production of desalination changes too, peaking at noon and being zero at night.

Figure 20 shows the fluctuations of the gain ratio in the desalination unit of different cases. Gain ratio (GOR) is the amount of seawater desalinated per unit motive steam used in the process, which represents how efficient the desalination unit is working. The higher this index is, the more efficient the system is. Changes in the motive steam mass flow are the main reason for this fluctuating behavior during the period in case 3 to 5. In case 2, since a constant flow is supplied from the turbine outlet stream as the motive steam, no changes in the gain ratio have happened.

The total distillation during the studied fifteen days is presented in Fig. 21. As expected, case 3, where both the heat from the turbine outlet stream and auxiliary burner exhaust gases is used to produce the motive steam used in the desalination unit, has the best performance in terms of desalinated water production. The second-best configuration is case 2, where the outlet turbine stream is directly used as the motive steam. Case 4, where only the waste heat from the auxiliary boiler is used to generate the motive steam used in the MED unit, has a considerably lower performance than the two other mentioned cases showing the heat wasted in the condenser is greater than the burner. And the last configuration, case 5, where the plants are assumed to be solar-only, produced the least amount of desalinated water during the 15-day period of study, which is predictable since no seawater is desalinated at night when there is no solar irradiation.

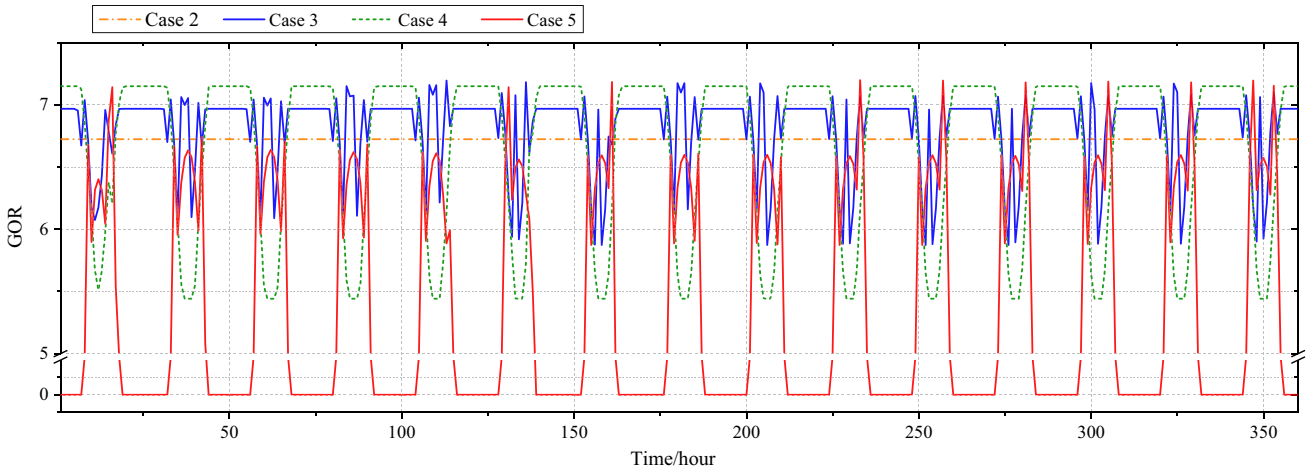

Fig. 20 Gain ratio of the MED unit in different case studies

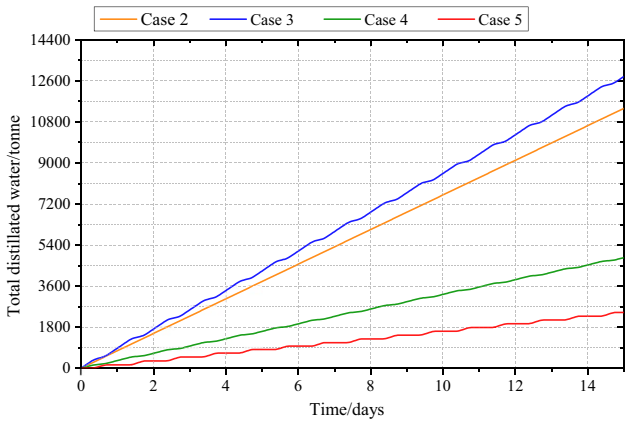

Fig. 21 Total distilled water in different cases of study

Table 7 Results of different scenarios for fifteen days of study

Case no	Average efficiency/%	Total fuel used/Tonne	Total CO_2 produced/Tonne	Total water desalinated/Tonne
Case 1	10.758	97.335	268.028	–
Case 2	10.754	97.335	268.028	11,389.083
Case 3	10.758	97.335	268.028	12,784.816
Case 4	10.758	97.335	268.028	4844.342
Case 5	11.084	–	–	2439.753

Finally, Table 7 details the performance of the five different cases of the plant in terms of average efficiency, total fuel consumption, total emission, and the total water desalinated during the 15 consecutive days of the operation of the plant. According to the table, cases 2, 3, and 4 display similar performance to the base power plant (case 1) in terms of efficiency, total fuel consumed, and the amount of CO_2 produced since only the waste heat is used for the addition of the desalination unit and the configuration of the system quite untouched. Case 5 shows higher efficiency compared to other cases because the irreversibility in the auxiliary boiler has a negative impact on the efficiency of the cycle, which is not relevant for case 5 since the system is power by only solar irradiation. In terms of the amount of distillate, case 2 shown the best performance, among others, with the average production of 9.864 kg s^{-1} desalinated water. The second-best configuration is when only using the heat wasted in the condenser (case3), which produced 8.787 kg s^{-1} of water averagely and case 4, when only the heat from boiler exhaust gases is used to generate the motive steam used in the desalination unit, has the lowest water production with only 3.737 kg s^{-1} of seawater desalination on average. In case 5, about 1.882 kg s^{-1} of distillate is produced, which shows the possibility of power-water cogeneration even in the solar-only configuration.

After the selection of the most efficient configuration for the heat recovery in the hybrid solar plant, an optimization process is applied to the selected scenario to find the optimum parameters of the plant. Thereby, case 3, which has the highest efficiency and distillation product, is optimized using the procedure described in Sect. 3.3. The aim of the two-objective optimization is maximizing the water distillation and energy efficiency of the power cycle. However, it is not possible to increase both of these objectives since increasing the energy efficiency results in less heat being wasted, thus decreasing the amount of generating motive steam and distilled water. As a result, the final optimum point is selected from the Pareto Frontier illustrated in Fig. 22.

The results of the two-objective optimization are summarized in Table 8. The results show that most of the improvement is in the distilled water (Y2), which is improved by

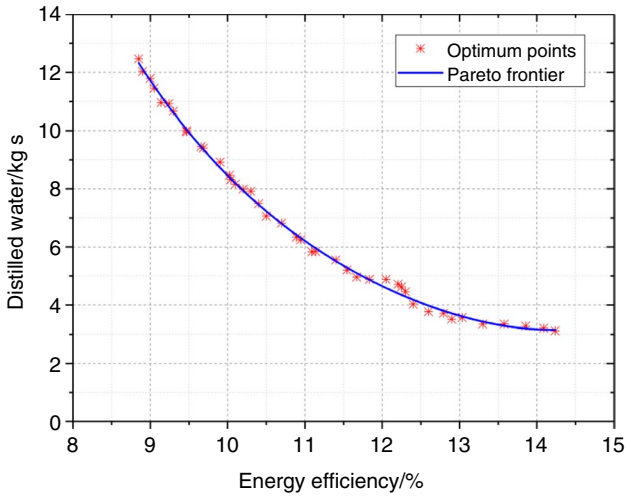

Fig. 22 Pareto front in the multi-objective optimization of case 3

Table 8 Results of the two-objective optimization

	Base values	Multi-objective optimization	Improvement
Decision variables			
X1	538.4 K	555.427	
X2	2100 kPa	1842.191	
X3	130 kPa	147.502	
X4	532.15 K	643.882	
X5	30 K	26.925	
Objective functions			
Y1	10.8811%	10.890	0.08%
Y2	5.8550 kg s^{-1}	6.332	8.14%

8.14%. The energy efficiency (Y1) of the plant is improved by 0.08% after applying the multi-objective optimization.

Conclusions

In this study, the Shiraz solar power plant has been analyzed as well as four different configurations of the hybridization of the plant with a desalination unit for cogeneration of power and water. A MED-TVC system is considered as the desalination unit, which has been implemented in different configurations to use the waste heat of the system to produce fresh water. This work investigated five different scenarios: first, the solar power plant without the desalination unit, second, using the desalination unit after the steam turbine to recover the waste heat from the turbine outlet stream, third, using both the waste heat in the condenser and exhaust gases of the boiler to generate the motive steam used in the MED-TVC unit, forth, using only the waste heat from the boiler's exhaust gases, and fifth, recovering the turbine outlet waste heat where the power plant is solar only, and there is no auxiliary boiler.

The results of the thermodynamic analysis show that all configurations have approximately similar efficiency of power generation, which is expectable since only the waste heat is used in the desalination unit. But the performance of the configurations differs in terms of freshwater production. case 3 ranks best in terms of water desalination with an average of 9.87 kg s^{-1} of distillation and 6.82 of gain ratio. The second best configuration is case 2, with 8.79 kg s^{-1} and 6.72 of freshwater production and GOR. Case 4 and 5 have the worst performance with only 3.74 and 1.88 kg s^{-1} of average production rate and 6.66 and 6.04 gain ratio.

The sensitivity analysis of the cycle shows that an electric efficiency of 14% can be achieved by increasing the turbine inlet temperature to 620 k and decreasing the turbine outlet pressure to 60 kPa. However, increasing the turbine outlet pressure had improved the performance of the desalination unit in case 3 since it increased the waste heat used in the MED-TVC unit while it had a negative impact on the water production in case 2 and 5 as it can cause a decrease in the entrained flow rate while increasing this pressure. The results show that changes in this pressure did not impact the water production performance in case 4 since only the waste heat from the boiler was used in this scenario.

The relation of gain ratio with the changes in top brine temperature and the number of effects is also investigated. The results show that by decreasing the top brine temperature and increasing the number of effects, higher gain ratios can be achieved. However, it should be considered that increasing the number of effects increases the specific heat transfer area too, which will increase the cost of the plant.

Also, each cycle is studied over a fifteen-day period to evaluate the performance of them under real conditions. While case 2 had the most stable performance in terms of the freshwater production and gain ratio, case 3 had the best average energy efficiency and distilled water between the investigated scenarios. The water production in case 3 during this time period was 12,784.816 tonne and 852.321 tonne per day on average. The CO_2 production of all cases is similar to each other and equal to 17.868 tonne per day. The total fuel used during this fifteen-day period is 97.335 tonne.

Finally, the selected scenario, case 3, which has the highest distillation and efficiency, is optimized using the genetic algorithm and a multi-objective approach. The results of the optimization show a 0.08% increase in energy efficiency while most of the improvement is in the freshwater production, increasing from 5.85 to 6.33 kg s^{-1} (8.14% improvement).

The results of this work show the possibility of recovering the waste heat of a small-scale solar power plant using

the desalination unit and improving the overall performance of the plant.

References

1. Arabkoohsar A, Andresen GBB. Supporting district heating and cooling networks with a bifunctional solar assisted absorption chiller. Energy Convers Manag. 2017;148:184–96. https://doi.org/10.1016/j.enconman.2017.06.004.
2. Alnaser WE, Alnaser NW. The status of renewable energy in the GCC countries. Renew Sustain Energy Rev. 2011;15:3074–98. https://doi.org/10.1016/j.rser.2011.03.021.
3. Arabkoohsar A, Andresen GBB. A smart combination of a solar assisted absorption chiller and a power productive gas expansion unit for cogeneration of power and cooling. Renew Energy. 2018;115:489–500. https://doi.org/10.1016/j.renene.2017.08.069.
4. Arabkoohsar A, Nami H. Thermodynamic and economic analyses of a hybrid waste-driven CHP–ORC plant with exhaust heat recovery. Energy Convers Manag. 2019;187:512–22. https://doi.org/10.1016/j.enconman.2019.03.027.
5. Sadi M, Arabkoohsar A. Modelling and analysis of a hybrid solar concentrating-waste incineration power plant. J Clean Prod. 2019;216:570–84. https://doi.org/10.1016/j.jclepro.2018.12.055.
6. Delyannis E-E. Status of solar assisted desalination: a review. Desalination. 1987;67:3–19. https://doi.org/10.1016/0011-9164(87)90227-X.
7. Sahoo U, Kumar R, Pant PC, Chaudhary R. Development of an innovative polygeneration process in hybrid solar-biomass system for combined power, cooling and desalination. Appl Therm Eng. 2017;120:560–7. https://doi.org/10.1016/j.applthermaleng.2017.04.034.
8. Mekhilef S, Saidur R, Safari A. A review on solar energy use in industries. Renew Sustain Energy Rev. 2011;15:1777–90. https://doi.org/10.1016/j.rser.2010.12.018.
9. Ahmed FE, Hashaikeh R, Hilal N. Solar powered desalination—technology, energy and future outlook. Desalination. 2019;453:54–76. https://doi.org/10.1016/J.DESAL.2018.12.002.
10. Kabeel AE, Abdelgaied M, Mahmoud GM. Performance evaluation of continuous solar still water desalination system. J Therm Anal Calorim. 2020. https://doi.org/10.1007/s10973-020-09547-5.
11. Khan MAM, Rehman S, Al-Sulaiman FA. A hybrid renewable energy system as a potential energy source for water desalination using reverse osmosis: a review. Renew Sustain Energy Rev. 2018;97:456–77. https://doi.org/10.1016/j.rser.2018.08.049.
12. Mohammadi K, Saghafifar M, Ellingwood K, Powell K. Hybrid concentrated solar power (CSP)-desalination systems: a review. Desalination. 2019;468:114083. https://doi.org/10.1016/j.desal.2019.114083.
13. Sahoo U, Kumar R, Pant PC, Chaudhury R. Scope and sustainability of hybrid solar–biomass power plant with cooling, desalination in polygeneration process in India. Renew Sustain Energy Rev. 2015;51:304–16. https://doi.org/10.1016/j.rser.2015.06.004.
14. Sankar D, Deepa N, Rajagopal S, Karthik KM. Solar power and desalination plant for carbon black industry: improvised techniques. Sol Energy. 2015;119:243–50. https://doi.org/10.1016/j.solener.2015.07.001.
15. Ghenai C, Merabet A, Salameh T, Pigem EC. Grid-tied and stand-alone hybrid solar power system for desalination plant. Desalination. 2018;435:172–80. https://doi.org/10.1016/j.desal.2017.10.044.
16. Sorgulu F, Dincer I. Design and analysis of a solar tower power plant integrated with thermal energy storage system for cogeneration. Int J Energy Res. 2019;43:6151–60.
17. Palenzuela P, Zaragoza G, Alarcón-Padilla DC, Guillén E, Ibarra M, Blanco J. Assessment of different configurations for combined parabolic-trough (PT) solar power and desalination plants in arid regions. Energy. 2011;36:4950–8. https://doi.org/10.1016/j.energy.2011.05.039.
18. Farsi A, Dincer I. Development and evaluation of an integrated MED/membrane desalination system. Desalination. 2019;463:55–68.
19. Trieb F, Nitsch J, Kronshage S, Schillings C, Brischke L-A, Knies G, Czisch G. Combined solar power and desalination plants for the Mediterranean region—sustainable energy supply using large-scale solar thermal power plants. Desalination. 2003;153:39–46. https://doi.org/10.1016/S0011-9164(02)01091-3.
20. Safari F, Dincer I. Development and analysis of a novel biomass-based integrated system for multigeneration with hydrogen production. Int J Hydrogen Energy. 2019;44:3511–26.
21. Hasan A, Dincer I. Assessment of an integrated gasification combined cycle using waste tires for hydrogen and fresh water production. Int J Hydrogen Energy. 2019;44:19730–41.
22. Ghasemiasl R, Javadi MA, Nezamabadi M, Sharifpur M. Exergetic and economic optimization of a solar-based cogeneration system applicable for desalination and power production. J Therm Anal Calorim. 2020. https://doi.org/10.1007/s10973-020-10242-8.
23. Hajibashi FA, Arabkoohsar A, Babaelahi M. Risk assessment, dynamic analysis and multi-objective optimization of a solar-driven hybrid gas/steam power plant. J Therm Anal Calorim. 2020. https://doi.org/10.1007/s10973-020-10221-z.
24. Lorente A, Bejan K, Al-Hinai AZ, Sahin BS. Yilbas, Constructal design of distributed energy systems: solar power and water desalination. Int J Heat Mass Transf. 2012;55:2213–8. https://doi.org/10.1016/j.ijheatmasstransfer.2012.01.020.
25. Mehrpooya M, Ghorbani B, Hosseini SS. Thermodynamic and economic evaluation of a novel concentrated solar power system integrated with absorption refrigeration and desalination cycles. Energy Convers Manag. 2018;175:337–56. https://doi.org/10.1016/j.enconman.2018.08.109.
26. Mata-Torres C, Escobar RA, Cardemil JM, Simsek Y, Matute JA. Solar polygeneration for electricity production and desalination: case studies in Venezuela and northern Chile. Renew Energy. 2017;101:387–98. https://doi.org/10.1016/j.renene.2016.08.068.
27. Coppitters D, Contino F, El-Baz A, Breuhaus P, De Paepe W. Techno-economic feasibility study of a solar-powered distributed cogeneration system producing power and distillate water: sensitivity and exergy analysis. Renew Energy. 2020;150:1089–97.
28. Casimiro S, Cardoso J, Alarcón-Padilla D-C, Turchi C, Ioakimidis C, Mendes JF. Modeling multi effect distillation powered by CSP in TRNSYS. Energy Procedia. 2014;49:2241–50. https://doi.org/10.1016/j.egypro.2014.03.237.
29. Mahfuz MH, Kamyar A, Afshar O, Sarraf M, Anisur MR, Kibria MA, Saidur R, Metselaar I. Exergetic analysis of a solar thermal power system with PCM storage. Energy Convers Manag. 2014;78:486–92.
30. Mosleh HJ, Ahmadi R. Linear parabolic trough solar power plant assisted with latent thermal energy storage system: a dynamic simulation. Appl Therm Eng. 2019;161:114204.
31. Baghernejad A, Yaghoubi M. Thermoeconomic methodology for analysis and optimization of a hybrid solar thermal power plant. Int J Green Energy. 2013;10:588–609.
32. Cengel YA, Boles MA. Thermodynamics: an engineering approach. Sea. 2002;1000:8862.

33. Vakilabadi MA, Bidi M, Najafi AF, Ahmadi MH. Energy, Exergy analysis and performance evaluation of a vacuum evaporator for solar thermal power plant zero liquid discharge systems. J Therm Anal Calorim. 2020;139:1275–90.
34. Acar MS, Arslan O. Energy and exergy analysis of solar energy-integrated, geothermal energy-powered organic rankine cycle. J Therm Anal Calorim. 2019;137:659–66.
35. Arabkoohsar A, Andresen GB. Dynamic energy, exergy and market modeling of a high temperature heat and power storage system. Energy. 2017. https://doi.org/10.1016/j.energy.2017.03.065.
36. Al-Mutaz IS, Wazeer I. Development of a steady-state mathematical model for MEE-TVC desalination plants. Desalination. 2014;351:9–18.
37. Barza A, Shourije SR, Pirouzfar V. Industrial optimization of multi-effect desalination equipment for olefin complex. J Therm Anal Calorim. 2020;139:237–49.
38. Carati A, Marino M, Brogioli D. Thermodynamic study of a distiller-electrochemical cell system for energy production from low temperature heat sources. Energy. 2015;93:984–93. https://doi.org/10.1016/j.energy.2015.09.108.
39. El-Dessouky HT, Ettouney HM. Fundamentals of salt water desalination. New York: Elsevier; 2002.
40. Ariafar K, Buttsworth D, Al-Doori G, Sharifi N. Mixing layer effects on the entrainment ratio in steam ejectors through ideal gas computational simulations. Energy. 2016;95:380–92. https://doi.org/10.1016/j.energy.2015.12.027.
41. Khan SU-D, Danish SN, Haider S, Khan SU-D. Theoretical calculation simulation studies of ABV nuclear reactor coupled with desalination system. Int J Energy Res. 2015;39:1554–63. https://doi.org/10.1002/er.3363.
42. You H, Han J, Liu Y. Performance assessment of a CCHP and multi-effect desalination system based on GT/ORC with inlet air precooling. Energy. 2019;185:286–98. https://doi.org/10.1016/j.energy.2019.06.177.
43. Babaelahi M, Rafat E, Mofidipour E. Emergy-based economic and environmental analysis and multi-objective optimization of a two-cascade solar gas turbine power plant. Sustain Prod Consum. 2019;20:165–77.
44. Dincer I, Rosen MA, Ahmadi P. Optimization of energy systems. New York: Wiley; 2017.
45. Niknia I, Yaghoubi M. Transient analysis of integrated Shiraz hybrid solar thermal power plant. Renew Energy. 2013;49:216–21.
46. Sadri S, Ameri M, Khoshkhoo RH. Multi-objective optimization of MED-TVC-RO hybrid desalination system based on the irreversibility concept. Desalination. 2017;402:97–108.